ISSN 0036-0236, Russian Journal of Inorganic Chemistry, 2011, Vol. 56, No. 1, pp. 93–98. © Pleiades Publishing, Ltd., 2011.
Original Russian Text © O.I. V'yunov, O.N. Gavrilenko, L.L. Kovalenko, S.A. Chernukhin, L.O. Vasilechko, S.D. Kobilyanskaya, A.G. Belous, 2011, published in Zhurnal Neorganicheskoi Khimii, 2011, Vol. 56, No. 1, pp. 97–102.

PHYSICAL METHODS OF INVESTIGATION

Intercalation Processes Influence the Structure and Electrophysical Properties of Lithium-Conducting Compounds Having Defect Perovskite Structure

O. I. V'yunov[a], O. N. Gavrilenko[a], L. L. Kovalenko[a], S. A. Chernukhin[b], L. O. Vasilechko[c], S. D. Kobilyanskaya[a], and A. G. Belous[a]

[a] *Vernadsky Institute of General and Inorganic Chemistry, National Academy of Sciences of Ukraine, Kiev, Ukraine*
[b] *Interagency Department of Electrochemical Power Production, National Academy of Sciences of Ukraine, Kiev, Ukraine*
[c] *Lviv Polytechnica National University, Ukraine*

Received April 30, 2009

Abstract—The structural features and electrophysical properties of lithium-conducting compounds having defect perovskite structure based on $Li_{0.5}La_{0.5}Nb_2O_6$ and $Li_{0.5}La_{0.5}TiO_3$ were studied using X-ray diffraction and synchrotron analyses, potentiometry, and complex impedance spectroscopy. Intercalated lithium was found to differently influence ion conductance in titanium- and niobium-containing materials. This difference was found to arise from the structural features of the materials. The systems studied have high chemical diffusion coefficients of lithium ($D^+_{Li} = 1 \times 10^{-6}$ cm^2/s for $Li_{0.5}La_{0.5}Nb_2O_6$ and $D^+_{Li} = 3.3 \times 10^{-7}$ cm^2/s for $Li_{0.5}La_{0.5}TiO_3$).

DOI: 10.1134/S0036023611010232

Lithium-conducting compounds are of great interest as materials for solid-state rechargeable lithium batteries having high energy contents and working voltages [1, 2]. Of such the materials, high room-temperature conductivity (on the order of 10^{-3} to 20^{-5} S/cm) is found in perovskite compounds (ABO_3), specifically, lithium lanthanum titanates $Li_{3x}La_{2/3-x}\square_{1/3-2x}TiO_3$ (LLTO) and lithium lanthanum niobates $Li_{3x}La_{2/3-x}\square_{4/3-2x}Nb_2O_6$ (LLNO), where $\square$ stands for a vacancy in sublattice A [3, 4]. In the structure of these materials, there are cationic vacancies distributed over sublattice A that influence lithium-ion conductance. The concentration variation of conductance in titanium-containing (LLTO) samples is described by a percolation model [5]. Conductance as a function of lithium concentration and vacancy concentration in the LLNO system was studied [6]. Use of the aforementioned systems as electrolytes in electrochemical engineering calls for studying the influence of lithium intercalation on the structure and properties of lithium-conducting materials.

In the LLTO system, studied were the existence fields and electrophysical properties of intercalated solid solutions [7, 8]. How unit cell parameters change upon intercalation was studied [9]. Proceeding from the obedience of conductance versus temperature in LLTO to the Vogel–Tammann–Fulcher law [10, 11], it is suggested that oxygen octahedra turn upon heating. Further, from dilatometric studies on $Li_{0.5}La_{0.5}TiO_3$ (LLTO with $x = 1/6$), it was inferred that a first-order phase transition can exist within the orthorhombic system in the temperature range of 880–915 K. From cyclic voltammograms [10], it was deduced that intercalation is a reversible reaction and occurs at potentials of about 1.5 V. Deintercalation can be accomplished by a chemical method, namely, by reaction with iodine in acetonitrile at 330 K for 72 h [13]. In the same work, deintercalation in perovskites led to Ti^{3+} oxidation accompanied by oxygen sorption from air and oxygen reduction to O^{2-} or Li_2O elimination.

Single-phase samples in the LLNO system were shown to exist when $0 \le x \le 0.06$. Cyclic voltammetry showed that lithium intercalation started at 1.75 V and was only partially reversible. The temperature variations of LLNO conductance were shown to obey an exponential law with the activation energy of conductance being 0.35 ± 0.03 eV for all samples.

The lithium amount increases in the course of intercalation, which can, on the one hand, decrease the amount of structural vacancies and, on the other, change the charge in the titanium (niobium) sublattice, namely reduce transition-metal ions to lower oxidation numbers. All the aforementioned circumstances can have a considerable effect on both the structural and the electrophysical properties of the systems under consideration. Therefore, it is of interest to study the properties of materials both after intercalation and after annealing intercalated samples in air, this annealing being accompanied by $Nb^{4+}(Ti^{3+})$ oxidation, as the chemical compositions of a sample can differ from its initial composition.

In light of the foregoing, this work was intended to study the structural and electrophysical characteristics of intercalated and air-annealed intercalated titanates and niobates having defect perovskite structures.

EXPERIMENTAL

The initial reagents used for the solid-phase synthesis of LLTO and LLNO samples were Li_2CO_3, La_2O_3, TiO_2, and Nb_2O_5 (all of high purity grade). Before use, La_2O_3, Li_2CO_3, and TiO_2 (Nb_2O_5) were calcined for 4 h at 1170, 870, and 670 K, respectively, to free them from trace water and adsorbed gases. Because of the high hygroscopicity of the components, they were weighed to prepare a batch immediately after having been calcined. Homogenizing milling was performed in a vibration mill by means of corundum milling bodies in aqueous solution for 4 h. A predried (at 370 K) batch was subjected to isothermal treatment at 1350–1490 K with an exposure time of 2 h. To analyze polycrystalline perovskite powders for lithium, a weighed portion of finely divided ceramics was admixed with a tenfold excess of $K_2S_2O_7$ and the mixture was alloyed for 24 h on a sand bath. The alloy was dissolved in acidified water. The solution was analyzed on an SP-9 PueUnicom atomic-absorption spectrometer. The determination error did not exceed 2%.

Products were identified by X-ray diffraction patterns recorded on DRON-4-07 (CuK_α radiation). Unit cell parameters were determined by the Rietveld full-profile analysis using X-ray diffraction and synchrotron data. Synchrotron patterns were obtained at the Max-Planck Institute for Chemical Physics of Solids (Dresden, Germany). Test samples for electrophysical studies were 12 mm in diameter and were compacted under 80 MPa/cm and sintered at 1520–1620 K. Sintered samples were cut into disks 1 mm thick. Lithium intercalation was carried out in a box filled with an inert atmosphere. The electrodes used were electron-beam-sputtered nickel (0.3–0.5 μm) and copper rods with lithium pressed on. Current was measured versus time in a potentiostatic mode (U = 0.1 V) on a PI-50-1 potentiostat. Electrophysical properties were studied for as-sintered samples, intercalated samples, and oxidized intercalated samples. Electrodes were formed by applying indium–gallium paste. Impedance studies were carried out in the range from 100 Hz to 1 MHz using a 1260A Impedance/Gain-Phase Analyzer (Solartron Analytical). The equivalent circuit and the values of its components were determined by means of the Frequency Response Analyser 4.7 program. Electronic conductance was derived from the voltage–current characteristics of test samples with blocking platinum microelectrodes using an Electrometer/High Resistance Meter 6517B (Keithley Instruments) digital electrometer [15].

RESULTS AND DISCUSSION

The test materials had as-batch compositions $Li_{0.2}La_{0.6}TiO_3$, $Li_{0.5}La_{0.5}Nb_2O_6$ and $Li_{0.32}La_{0.56}Nb_2O_6$. The high-temperature synthesis was accompanied by ~30 mol % loss of lithium and attendant generation of oxygen vacancies. Therefore, the actual compositions of the materials used to study intercalation may be written as $Li_{0.35}La_{0.5}TiO_{3-\delta}$, $Li_{0.14}La_{0.5}TiO_{3-\delta}$, $Li_{0.35}La_{0.5}Nb_2O_{6-\delta}$, and $Li_{0.22}La_{0.5}Nb_2O_{6-\delta}$, respectively, in agreement with previous results [16, 17]. Thus, lithium intercalation is performed into lithium-deficient samples. In what follows, as-batch compositions are given.

Figure 1 represents the plot of current strength I as a function of time τ measured in the potentiostatic mode (U = 0.1 V) during lithium intercalation into polycrystalline samples of as-batch compositions $Li_{0.5}La_{0.5}Nb_2O_6$ and $Li_{0.5}La_{0.5}TiO_3$. The plots feature three portions. One portion, at 7 and 21 min since the voltage application moment for $Li_{0.5}La_{0.5}Nb_2O_6$ and $Li_{0.5}La_{0.5}TiO_3$, respectively, is due to the / counterflow of lithium in the Li-electrode–polycrystalline sample direction until the diffusion interfaces join.

Inasmuch as charge transfer during the measurements had a diffusion component and a drift component, charge transfer was analyzed as effected by the voltage applied. The mean-square displacement L of particle during time τ_{diff} was related to the chemical diffusion coefficient through the Einstein fundamental relation: $L^2 = 6D\tau_{diff}$ [18].

Assuming that the test sample is homogeneous, we may write the equation for lithium ion drift velocity as $v = \mu E$, where μ is the charge carrier mobility and E is the electric field strength ($E = U/L$). Proceeding from the well-known relationship for diffusion and drift coefficients $D/\mu = kT/e$, where k is the Boltzmann constant, T is temperature, e is electron charge [19], and using the Einstein relationship, we may estimate the ratio between diffusion and drift times as $\tau_{diff}/\tau_{dr} = Ue/6kT = 6 \times 10^9$. This estimate shows that charge carrier transport by drift under a voltage of 0.1 V is far slower than transport by diffusion; that is, the drift component of charge transfer may be ignored. Therefore, we admit that, when lithium electrodes are applied to the two sides of a sample, the lithium diffusion interfaces join at a distance of about one-half the thickness of the polycrystalline sample, i.e., one-half the distance between the electrodes. The time taken to pass this distance is a measure of the velocity of the diffusion interfaces. Therefore, the lithium chemical diffusion coefficient D_{Li^+} was determined from the Einstein relation on the assumption that L corresponds to one-half the thickness of a polycrystalline sample.

The values of 1×10^{-6} and 3.3×10^{-7} cm^2/s were calculated by this relationship for D_{Li^+} in $Li_{0.5}La_{0.5}Nb_2O_6$ and $Li_{0.5}La_{0.5}TiO_3$, respectively. The classical method of galvanostatic titration used for calculating D_{Li^+} in

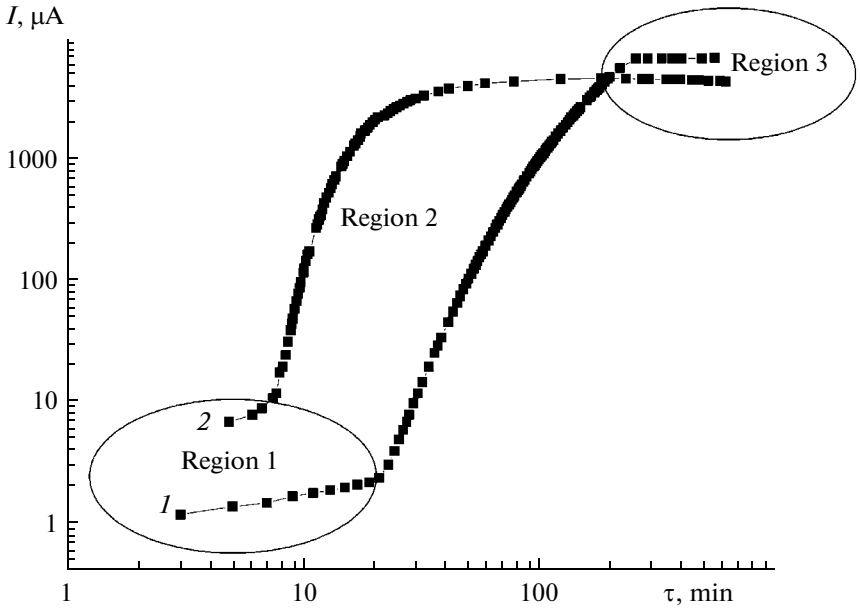

Fig. 1. I–τ potentiostatic curves ($U = 0.1$ V) recorded upon lithium intercalation into (*1*) $Li_{0.5}La_{0.5}Nb_2O_6$ and (*2*) $Li_{0.5}La_{0.5}TiO_3$ samples.

LLTO gave similar values: $D_{Li^+} = 10^{-6.5}$ to 10^{-7} cm^2/s [7]. Therefore, the approach to calculating D_{Li^+} used in this work may be regarded as adequate enough.

In the first portion (Fig. 1), the rise in conductance is due to the shrinkage of an ionic conductance region on account of an expanding near-electrode region where both ionic and electronic components contribute to the conductance. The increase in electronic component in the near-electrode region results from the redox processes that occur during intercalation and yield Ti^{3+} and Nb^{4+}:

$$Li - e^- \longrightarrow Li^+ + e^-,$$

$Ti^{4+} + e^- \longrightarrow Ti^{3+}$ in lithium lanthanum titanates,

$Nb^{5+} + e^- \longrightarrow Nb^{4+}$ in lithium lanthanum niobates.

The presence of Ti^{3+} and Nb^{4+} paramagnetic centers, which are responsible for blackening of the samples, is verified by EPR spectroscopy [20, 21].

In the second portion, the current considerably increases with time (Fig. 1) because of a considerable increase in the electronic contribution to the overall conductance. The diffusion and reduction of the transition-metal ions continue in the region where the diffusion interfaces meet.

In the third portion (Fig. 1), I–τ curves acquire saturation, proving that lithium ion diffusion and the attendant Ti^{4+} and Nb^{5+} reduction is complete over the entire bulk of the sample.

For reducing the contribution to electronic conductance caused by the presence of Ti^{3+} and Nb^{4+} in the intercalated samples, they were in addition heat treated in air at 300–870 K for 6 h. As the heat treatment temperature increased, the resistivity of the intercalated samples shifted up; saturation was acquired at about 870 K. The samples, being dark because of reduced titanium or niobium ions, grew lighter over the entire bulk (as monitored visually over the cleavage) due to the aforementioned redox processes:

$$O_2 + 4e^- \longrightarrow 2O^{2-},$$

$Ti^{3+} - e^- \longrightarrow Ti^{4+}$ in lithium lanthanum titanates,

$Nb^{4+} - e^- \longrightarrow Nb^{5+}$ in lithium lanthanum niobates.

After lithium intercalation and annealing in air at temperatures at which there is no noticeable lithium loss, the deficit of lithium relative to stoichiometry was as low as 2%; that is, the solid solution composition may be written as $Li_{0.49}La_{0.5}TiO_{3-\gamma}$, $Li_{0.19}La_{0.6}TiO_{3-\gamma}$, $Li_{0.49}La_{0.5}Nb_2O_{6-\gamma}$, and $Li_{0.31}La_{0.56}Nb_2O_{6-\gamma}$. Intercalation practically compensates for the lithium deficit caused by lithium volatility.

Tables 1 and 2 display the structural parameters of initial (as-sintered) samples, lithium-intercalated samples, and intercalated samples after oxidative heat treatment for LLTO and LLNO systems, respectively. The unit cell parameters of intercalated samples for the systems under consideration differ considerably from the parameters of the non-intercalated samples. Specifically, intercalation considerably increases the unit cell volume, presumably because of the appearance of Ti^{3+} and Nb^{4+} ions, whose ionic radii are greater than Ti^{4+} and Nb^{5+} ionic radii, respectively, as well as partial filling of vacant positions by lithium ions which are intercalated into the perovskite structure.

Table 1. Structural parameters of samples of the $Li_{3x}La_{2/3-x}TiO_3$ system

Composition	$Li_{0.2}La_{0.6}TiO_3$			$Li_{0.5}La_{0.5}TiO_3$		
	as-sintered samples	after lithium intercalation	after oxidation of intercalated samples	as-sintered samples	after lithium intercalation	after oxidation of intercalated samples
Unit cell parameters, space group *R*-3*c*						
a, Å	5.4829(3)	5.4912(6)	5.4832(3)	5.475(5)	5.483(9)	5.476(4)
c, Å	13.414(1)	13.398(2)	13.417(1)	13.41(3)	13.43(5)	13.41(2)
V, Å^3	349.23(4)	349.87(8)	349.35(4)	348.2(8)	349.8(15)	348.3(6)
Coordinates of ions						
O: *x*/*a*	0.473(4)	0.520(8)	0.479(5)	0.467(3)	0.531(5)	0.463(3)
Reliability factor						
R_B, %	6.5	9.2	6.6	9.2	9.6	8.3
R_f, %	6.0	8.2	6.4	7.4	6.7	7.4

Note: Ionic positions:La (6a) 0 0 1/4; Li (18d) ½ 0 0; Ti (6b) 0 0 0; O (18e) *x* 0 ¼.

Table 2. Structural parameters of samples of the $Li_{3x}La_{2/3-x}Nb_2O_6$ system

Composition	$Li_{0.32}La_{0.56}Nb_2O_6$			$Li_{0.5}La_{0.5}Nb_2O_6$		
	as-sintered samples	after lithium intercalation	after oxidation of intercalated samples	as-sintered samples	after lithium intercalation	after oxidation of intercalated samples
Unit cell parameters, space group, *P*4/*mmm*						
a, Å	3.897(1)	3.908(2)	3.9057(5)	3.898(3)	3.9079(6)	3.903(3)
c, Å	7.893(2)	7.823(4)	7.821(1)	7.856(1)	7.829(1)	7.829(2)
V, Å^3	120.29(5)	120.63(9)	120.31(3)	119.4(1)	120.04(4)	119.3(1)
Coordinates of ions						
Nb: *z*/*c*	0.2625(9)	0.253(2)	0.2543(9)	0.252(1)	0.249(2)	0.250(1)
O_3: *z*/*c*	0.226(5)	0.205(5)	0.191(2)	0.215(3)	0.206(8)	0.220(5)
Reliability factor						
R_B, %	8.1	9.5	8.4	9.6	9.2	6.6
R_f, %	6.5	6.5	7.2	7.4	8.9	5.3

Note: Ionic positions: La (1a) 0 0 0; Nb (2t) ½ ½ *z*; O_1 (1f) ½ ½ 0; O_2 (1h) ½ ½ ½; O_3 (2s) ½ 0 z; O_4 (2r) 0 ½ *z*. Vacancy positions (1c) 0 0 ½.

The unit cell volume increases both in low-lithium samples ($Li_{0.2}La_{0.6}TiO_3$ and $Li_{0.32}La_{0.56}Nb_2O_6$) and in samples having compositions near the solid-solution boundary ($Li_{0.5}La_{0.5}TiO_3$ and $Li_{0.5}La_{0.5}Nb_2O_6$). The oxidation of intercalated samples in the systems under study decreases the unit cell volume compared to the intercalated samples (Tables 1, 2) because of the degree of oxidation of Ti^{3+} and Nb^{4+} increasing to Ti^{4+} and Nb^{5+}, respectively. The unit cell volume of the oxidized samples becomes equal to the unit cell volume in the samples before intercalation.

Figure 2 displays unit cell volume versus temperature plots for the materials under study plotted by the results of synchrotron studies. The trends of the plots signify the nonoccurrence of structural phase transitions in the system over wide temperature ranges.

Figure 3 displays the results of the complex impedance study of lithium-conducting titanate and niobate samples before and after intercalation and after oxidative heat treatment. The resistance of intercalated lithium lanthanum titanate and lithium lanthanum niobate (curves *2*) is far lower than for the as-sintered

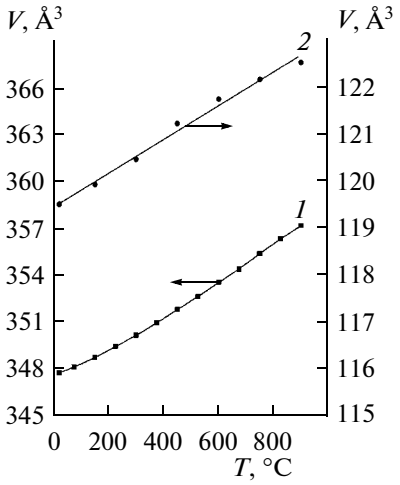

Fig. 2. Unit cell volume of (*1*) $Li_{0.5}La_{0.5}TiO_3$ and (*2*) $Li_{0.5}La_{0.5}Nb_2O_6$ intercalated samples after heat treatment in air for 6 h.

samples (curves *1*), which is explained by a considerable electronic term (Table 3) arising from the reduction of the transition-metal (titanium, niobium) ions during intercalation. The electrophysical properties of lithium-conducting ceramics after oxidation (curves *3*) are different. In the titanium-containing sample, the resistance shifts up relative to the as-sintered (non-intercalated) ceramics, whereas intercalated lithium-containing lanthanum niobate after oxidation has a lower resistance than before intercalation.

The aforementioned distinctions in electrophysical properties may arise from the structural perovskite features of the systems under consideration, primarily in the lanthanum (lithium) sublattice. In the $Li_{3x}La_{2/3-x}\square_{1/3-2x}TiO_3$ structure with $3x = 0.5$, ion transport is hindered by the nonexistence of free vacancies for lithium ions to migrate. Such vacancies, however, appear upon sintering on account of the considerable lithium loss, and the material acquires lithium conductance. Vacant positions are filled in upon intercalation to reduce lithium-ion conductance and enhance electronic conductance. Upon oxidation, the electronic conductance term decreases as a result of reduction ($Ti^{3+} - e^- \longrightarrow Ti^{4+}$).

In $Li_{3x}La_{2/3-x}\square_{4/3-2x}Nb_2O_6$ where $3x = 0.5$, there are a great many free vacancies. Considerable lithium losses are also observed in this system upon sintering to be then compensated by intercalation. However, a further increase in lithium content does not occur, as in a crystal there is no possibility of balancing the excess charge that could have been inserted by subsequent lithium intercalation. For this reason, a considerable amount of vacancies is saved in an intercalated LLNO sample with $3x = 0.5$ after the intercalation is over, obviously enhancing intercalated lithium ion transport in this system, whereas the LLTO system having a relatively lower amount of vacancies is less favorable

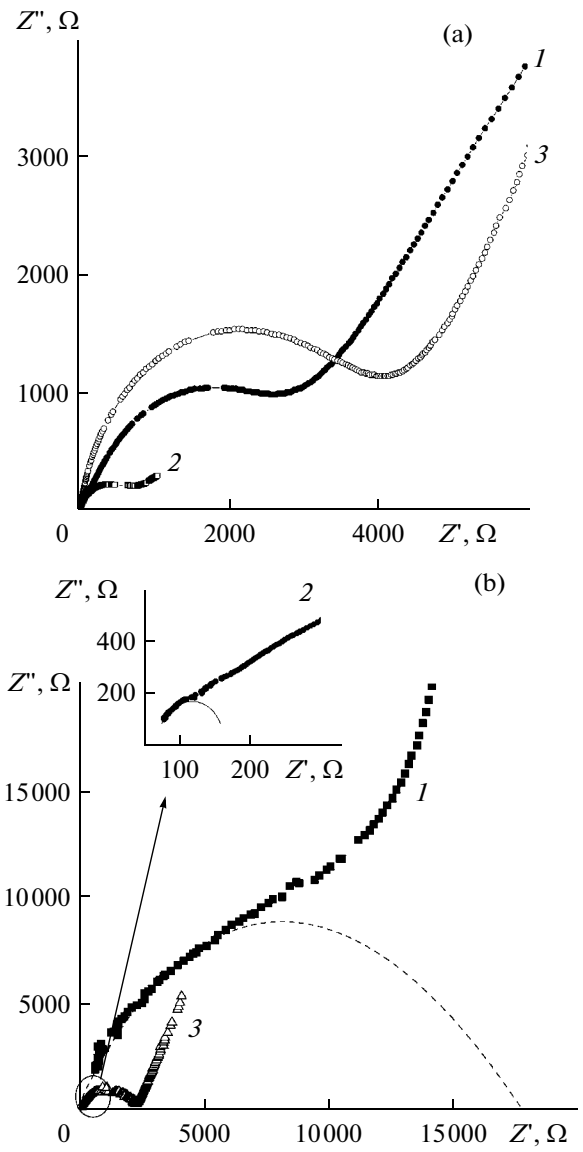

Fig. 3. Complex impedance curves for (a) $Li_{0.5}La_{0.5}TiO_3$ and (b) $Li_{0.5}La_{0.5}Nb_2O_6$ ceramics: (*1*) as-sintered, (*2*) lithium-intercalated, and (*3*) the same after oxidation. $T = 320$ K.

for the migration of ions additionally intercalated into the structure, partially blocking these ions in the perovskite positions.

In summary, we have studied lithium intercalation into polycrystalline samples of lithium-conducting lanthanum titanates and niobates having defect perovskite structures. We have shown that $Li_{0.5}La_{0.5}Nb_2O_6$ and $Li_{0.5}La_{0.5}TiO_3$ have high lithium chemical diffusion coefficients ($D_{Li^+} = 1 \times 10^{-6}$ and 3.3×10^{-7} cm^2/s, respectively).

We have studied how intercalation influences the structural parameters and electrophysical properties of lithium-conducting systems. The change in unit cell volume upon intercalation and upon oxidation of

Table 3. Electron and ion conductance (σ) in the perovskites studied

σ, S/cm^{-1}	As-sintered sample	After lithium intercalation	After oxidation of intercalated sample
	$Li_{0.5}La_{0.5}TiO_3$		
Electronic	1.1×10^{-9}	2.4×10^{-5}	1.3×10^{-9}
Ionic	3.1×10^{-5}	1.0×10^{-4}	1.9×10^{-5}
	$Li_{0.5}La_{0.5}Nb_2O_6$		
Electronic	1.1×10^{-9}	2.0×10^{-5}	1.5×10^{-9}
Ionic	0.5×10^{-5}	4.0×10^{-4}	3.8×10^{-5}

intercalated samples has been shown to arise primarily from redox processes influencing the average ion size in the titanium (niobium) sublattice) in perovskite structures.

We have shown that the existence of a plurality of vacancies and structural migration channels in the niobium-containing system enhance intercalated lithium ion transport in lithium-conducting lanthanum niobate. Ion conductance values in lithium-intercalated LLNO after oxidative heat treatment are far higher than in the as-sintered sample.

REFERENCES

1. P. P. Prosini, R. Mancini, L. Petrucci, et al., Solid State Ionics **144**, 185 (2001).
2. V. D. Prisyazhnyi, Visn. Kharkiv. Nats. Univ. Khim., issue 12(35), No. 648, 21 (2005).
3. A. G. Belous, G. N. Novitskaya, S. V. Polyanetskaya, and Yu. I. Gornikov, Izv. Akad. Nauk SSSR, Ser. Neorg. Mater. **23** (3), 470 (1987).
4. A. G. Belous, G. N. Novitskaya, S. V. Polyanetskaya, and Yu. I. Gornikov, Zh. Neorg. Khim. **32** (2), 283 (1987).
5. A. Rivera, C. León, J. Santamaría, et al., Chem. Mater. **14** (12), 5148 (2002).
6. A. Belous, E. Paskova, O. Gavrilenko, et al., J. Eur.. Ceram. Soc. **24**, 1301 (2004).
7. P. Birke, S. Scharner, R. A. Huggings, and W. Weppner, J. Electrochem. Soc. **144**, L167 (1997).
8. C. H. Chen and K. Amine, Solid State Ionics **144**, 51 (2001).
9. Y.-J. Shan, L. Chen, Y. Inaguma, et al., J. Power Sources **54**, 397 (1995).
10. O. Bohnke, C. Bohnke, and J. L. Fourquet, Solid State Ionics **91**, 21 (1996).
11. A. Belous, O. Yanchevskiy, O. V'yunov, et al., Chem. Mater. **16**, 407 (2004).
12. E. A. Fortal'nova, Candidate's Dissertation in Chemistry (Moscow, 2006).
13. M.-F. García, N. Fernández, K. Borrego, et al., J. Eur. Ceram. Soc. **25**, 729 (2005).
14. S. García-Martín, J. M. Rojo, H. Tsukamoto, et al., Solid State Ionics **116**, 11 (1999).
15. S. Lübke and H. D. Wiemhöfer, Solid State Ionics **117**, 229 (1999).
16. G. Emery, G. Y. Buzare, O. Bahnke, and G. L. Fourquet, Solid State Ionics **99**, 41 (1997).
17. A. G. Belous, O. N. Gavrilenko, E. V. Pashkova, et al., Neorg. Mater. **40** (8), 993 (2004).
18. L. Kavan, J. Procházka, T. M. Spitler, et al., J. Electrochem. Soc. **150** (7), A1000 (2003).
19. P. Kofstad, *Nonstoichiometry, Diffusion and Electrical Conductivity in Binary Metal Oxides* (Wiley, New York, 1972; Moscow, 1975).
20. V. V. Laguta, A. M. Slipenyuk, I. P. Bikov, et al., J. Appl. Phys. **97**, 073707 (2005).
21. V. N. Fedotov, N. S. Garif'yanov, and B. M. Kozyrev, Dokl. Akad. Nauk SSSR **145** (6), 578 (1962).